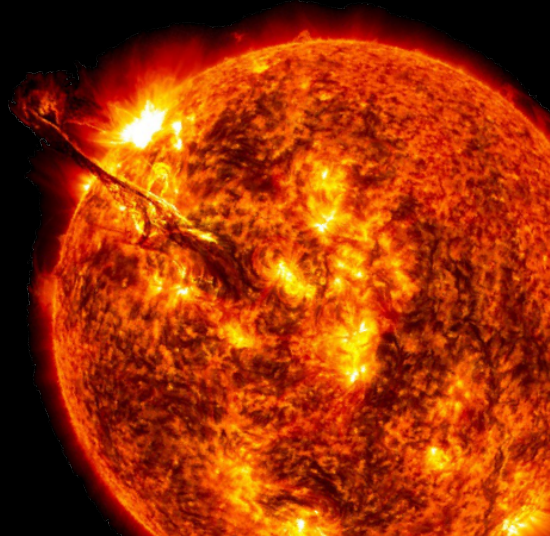
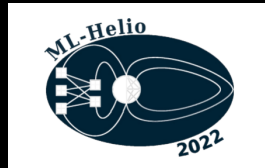


Farnet-II

Application of Convolutional LSTM and attention mechanisms to solar far-side activity detection

E. G. Broock (1,2), T. Felipe (1,2), A. Asensio Ramos (1,2)
(1) Instituto de Astrofísica de Canarias; (2) Universidad de La Laguna



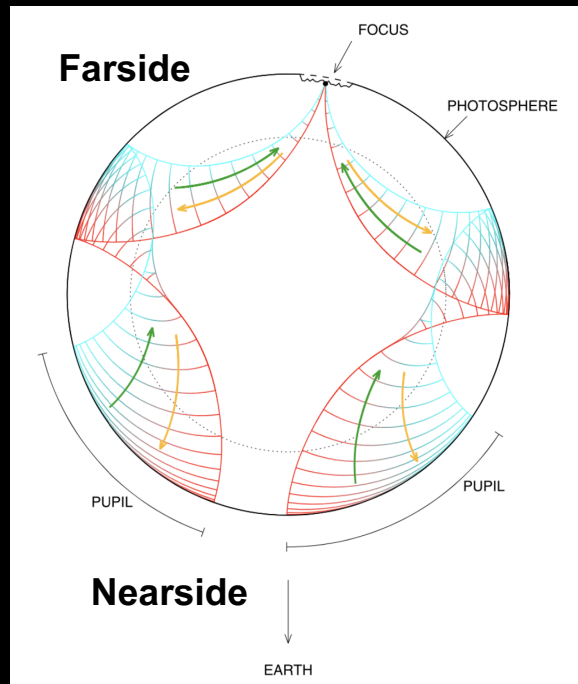


Content

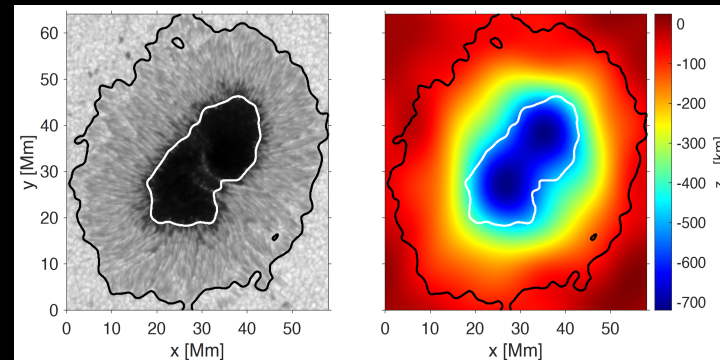
- 1. Farside activity detection**
- 2. FarNet**
- 3. FarNet-II**
- 4. Cross-validation study**
- 5. Ablation study**
- 6. Open work and conclusions**

Farside activity detection

Farside holography: phase-sensitive holography applied to the farside. Relies on refraction of acoustic waves (2.5mHz-4.5mHz). Active regions on the farside produce a phase-shift on the traveling waves.

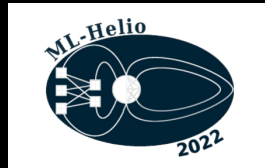


Wilson depression: Waves reflected lower than expected. Time-shift produces phase-shift.



Lindsey, C. & Braun, D. C. 2000b, Science, 287, 1799

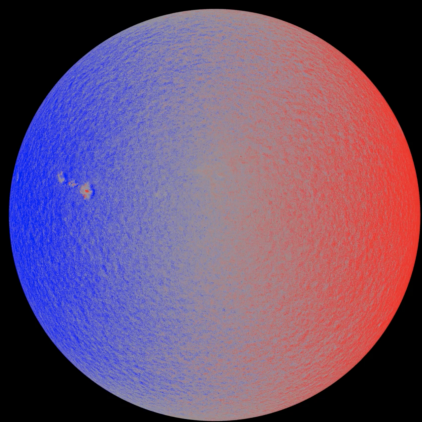
Löptien, B. et al
2018, A&A,
619, A42



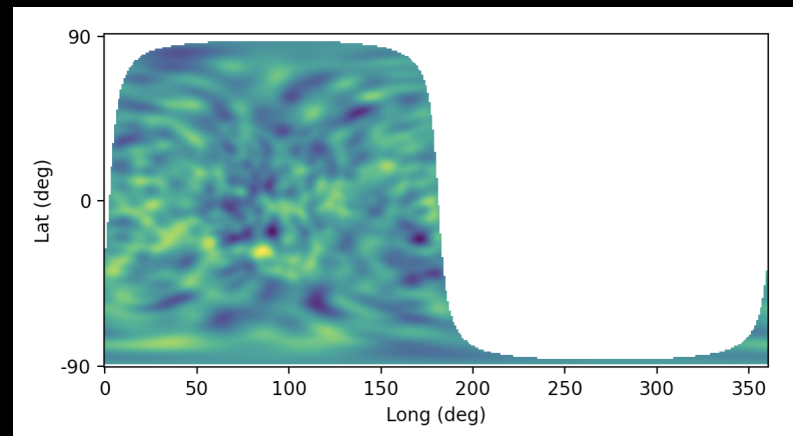
Farside activity detection

Standard method: use of Dopplergrams to construct farside phase-shift maps.

Source: NASA/GSFC/SDO

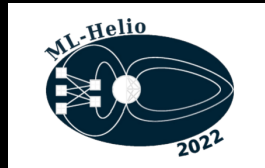


P-S map 1 June 2016. Source:
<http://isoc.stanford.edu/ajax/lookdata.html>



NS Dopplergrams
(31 h data)

FS Phase-shift maps
(24 h data)



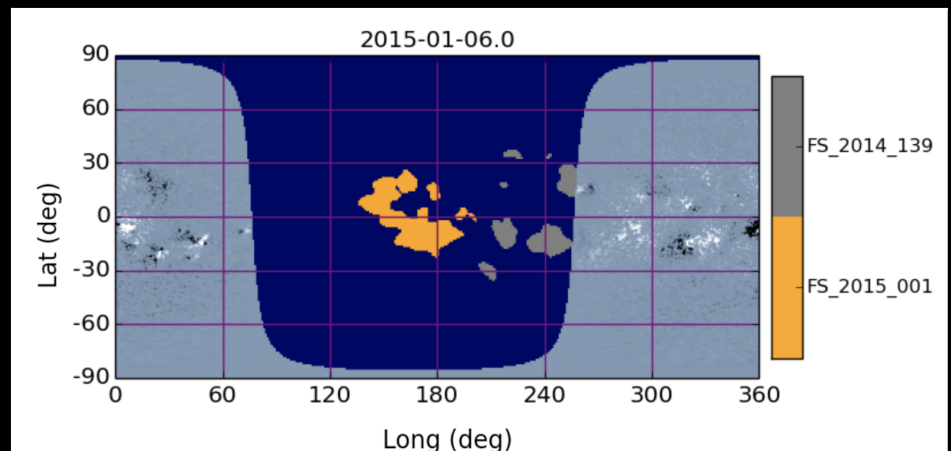
Farside activity detection

Standard method: filtering of phase-shift maps to generate actual detections.

Data product: 5 days cumulative Carrington phase-shift maps, computed from 24h phase-shift maps from HMI Doppler observations.

$\Delta\phi < -0.085$ rad (~ 4 s)

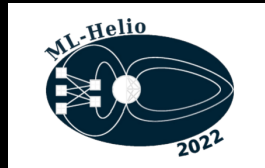
Seismic Strength (S): $S = \int_A \Delta\phi$



Strong active regions prediction from SSMS. 6 January 2015.

Source: <http://jsoc.stanford.edu/data/farside/>

SAR if $S > 400$

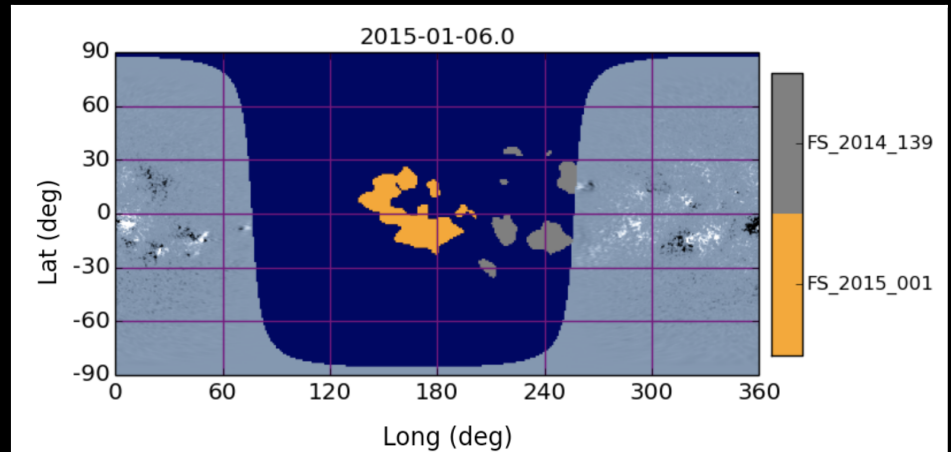


Farside activity detection

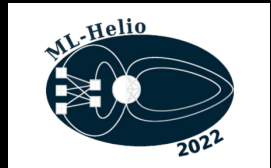
SAR if S>400

Only strong AR with great acoustic signatures can be reliably detected.

High signal-to-noise ratio needed.

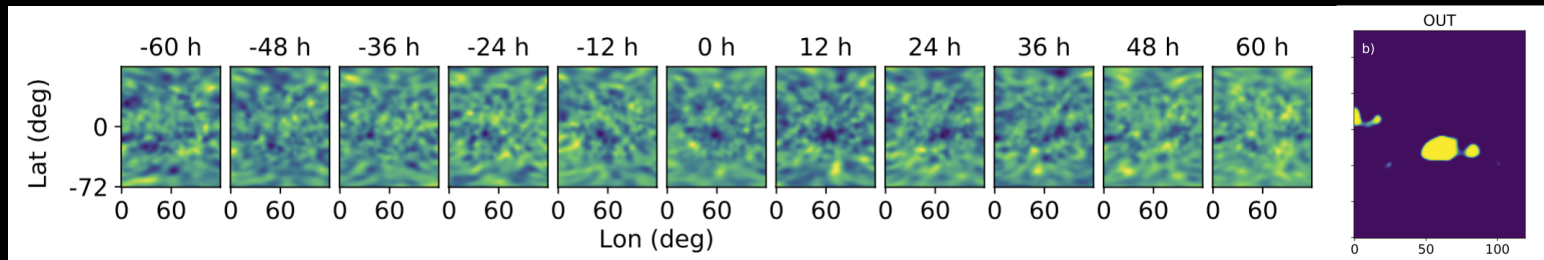


Strong active regions prediction from SSMS. 6 January 2015.
Source: <http://jsoc.stanford.edu/data/farside/>

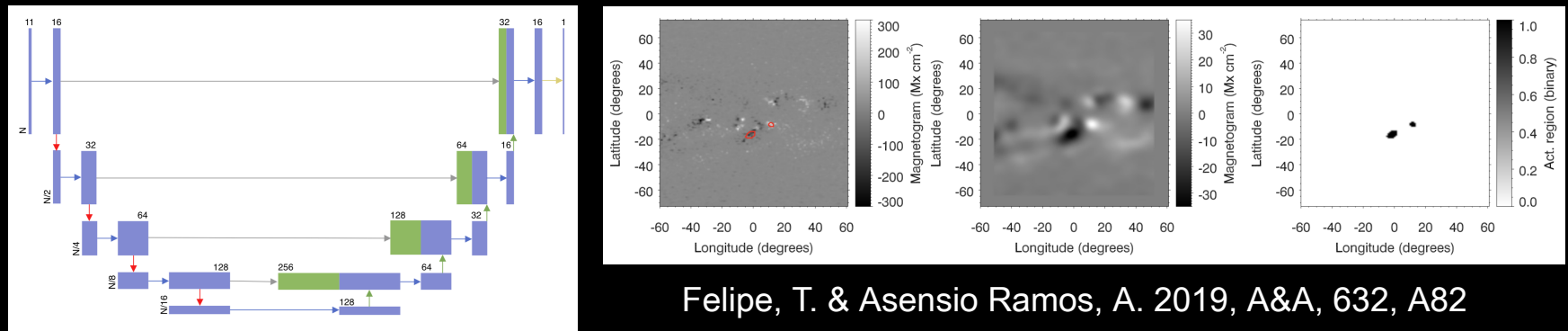


FarNet

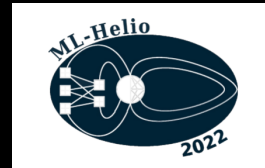
Overview: BCE loss, 300 epochs, BS 30, LR 3×10^{-4}



Broock, E. G., Felipe, T., & Asensio Ramos, A. 2021, Astronomy & Astrophysics, 652, A132

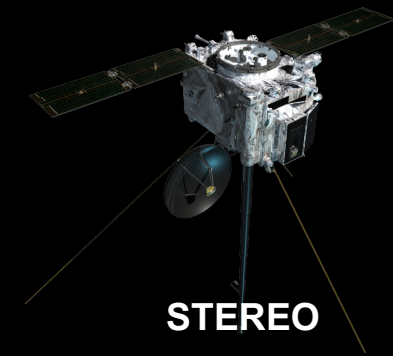
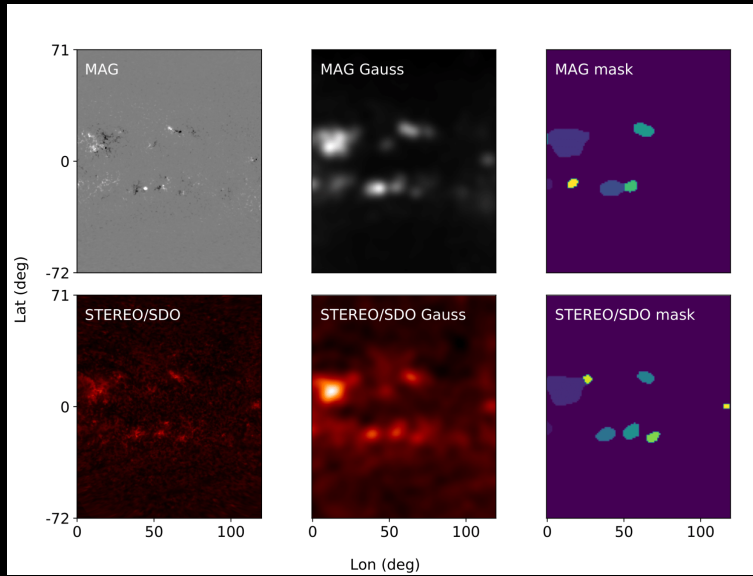


Felipe, T. & Asensio Ramos, A. 2019, A&A, 632, A82



FarNet

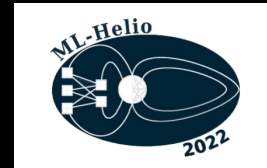
Overview:



47%
IMPROVEMENT

	Detections	False Positives
SS $S > 400$	1334	52 (3.75%)
NN $P_i > 113$	1958	76 (3.74%)

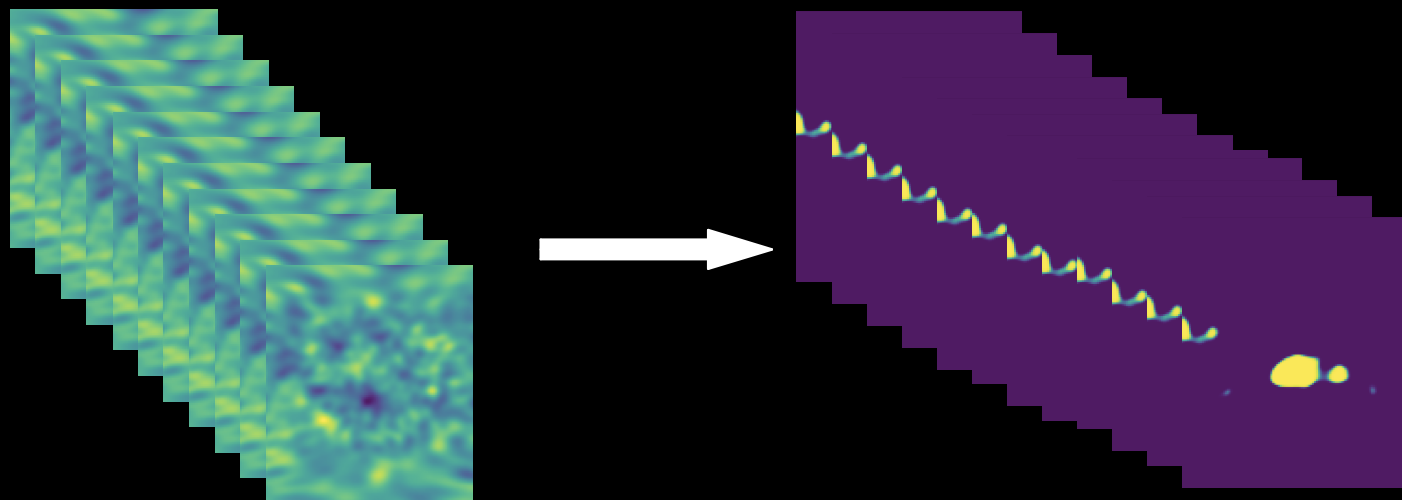
Broock, E. G., Felipe, T., & Asensio Ramos, A. 2021, *Astronomy & Astrophysics*, 652, A132



FarNet-II

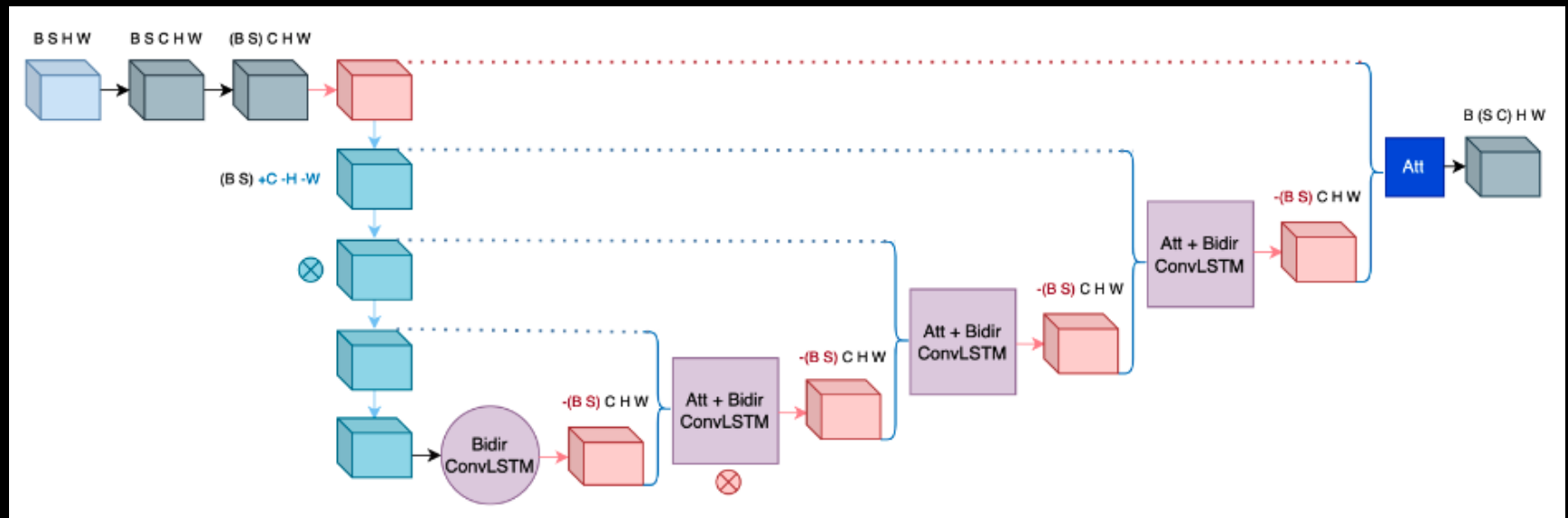
Aim: further improve FarNet's capabilities:

- Improve **temporal coherence** of the predictions.
- Having **one prediction for each input map** instead of for the central date.
- Improve the **superposition** of network outputs and **STEREO EUV masks**.

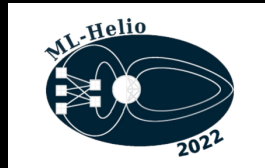


FarNet-II

Architecture: similar to FarNet but with new tools including **convolutional LSTM modules** and **attention mechanisms**.



Brock, E. G., Asensio Ramos, A. & Felipe, T., 2022, (in preparation)

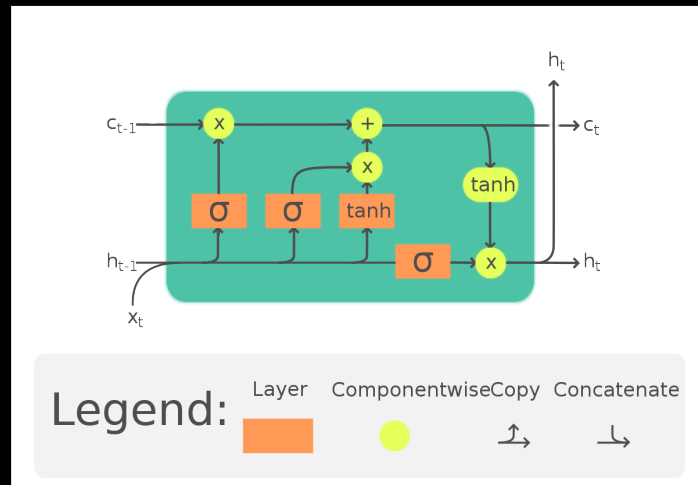


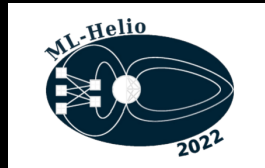
FarNet-II

Long-Short Term Memory (LSTM): recurrent machine learning mechanism used to work with time-series of data.

Similar to an RNN but avoid the vanishing gradient problem.

Uses information of previous inputs to compute current output. Information moduled by input, forget and output gates, using sigmoid functions.





FarNet-II

LSTM mainly used for translation.

Input has to be flattened before going into the module.

For computer vision this means losing spatial information.

Development of convolutional LSTM (Shi et al. 2015) to leverage LSTM capabilities while retaining spatial information.

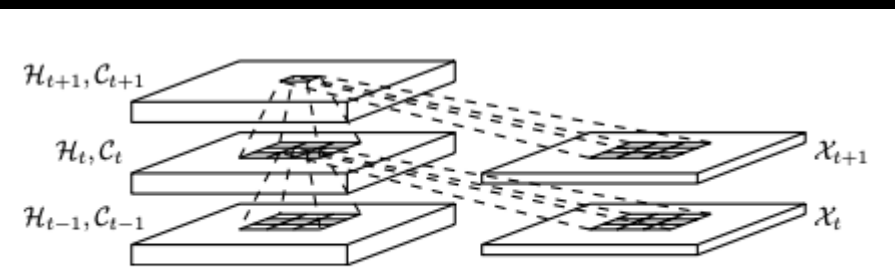
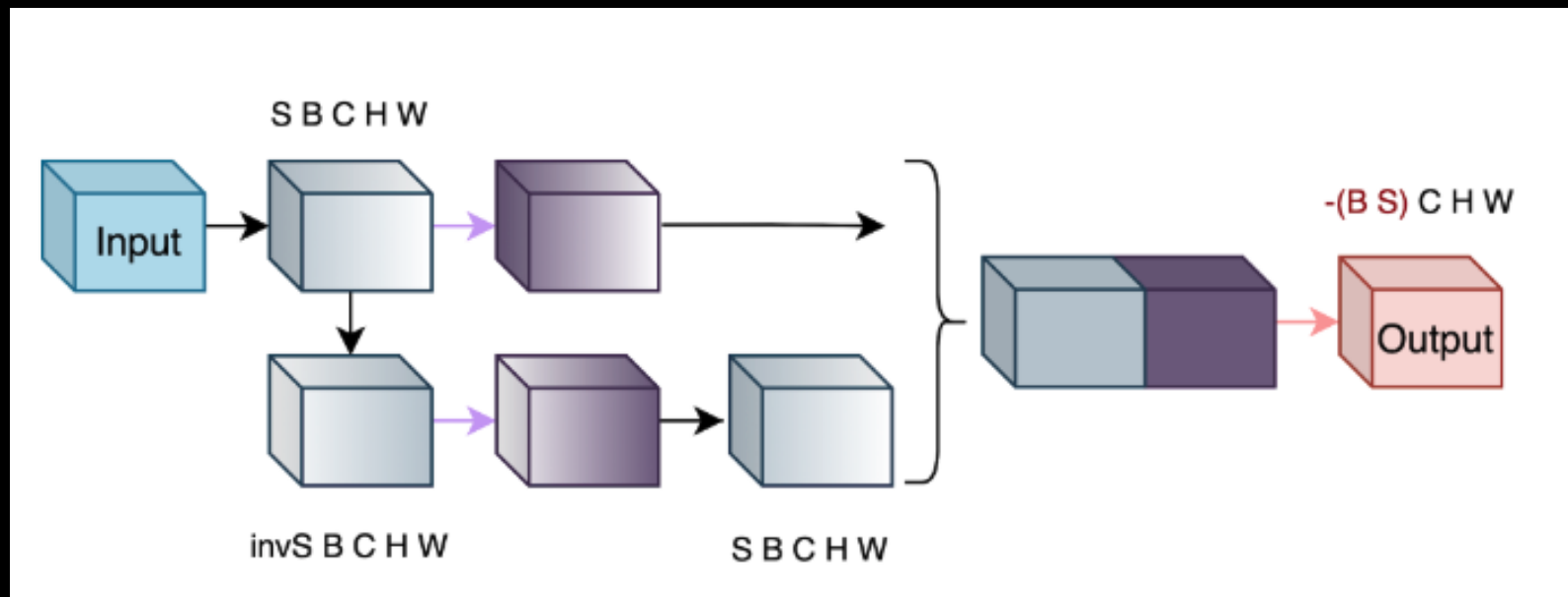


Figure 2: Inner structure of ConvLSTM

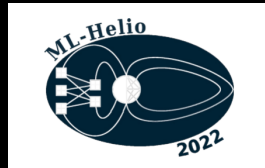
X. Shi, Z. Chen, H. Wang, D. Y. Yeung, W. K. Wong, and W. C. Woo, Advances in Neural Information Processing Systems, vol. 2015-January, pp. 802–810, 2015.

FarNet-II

Bidirectional use of ConvLSTM module: inversion of input and application of ConvLSTM to each copy, re-inversion, concatenation and convolution.

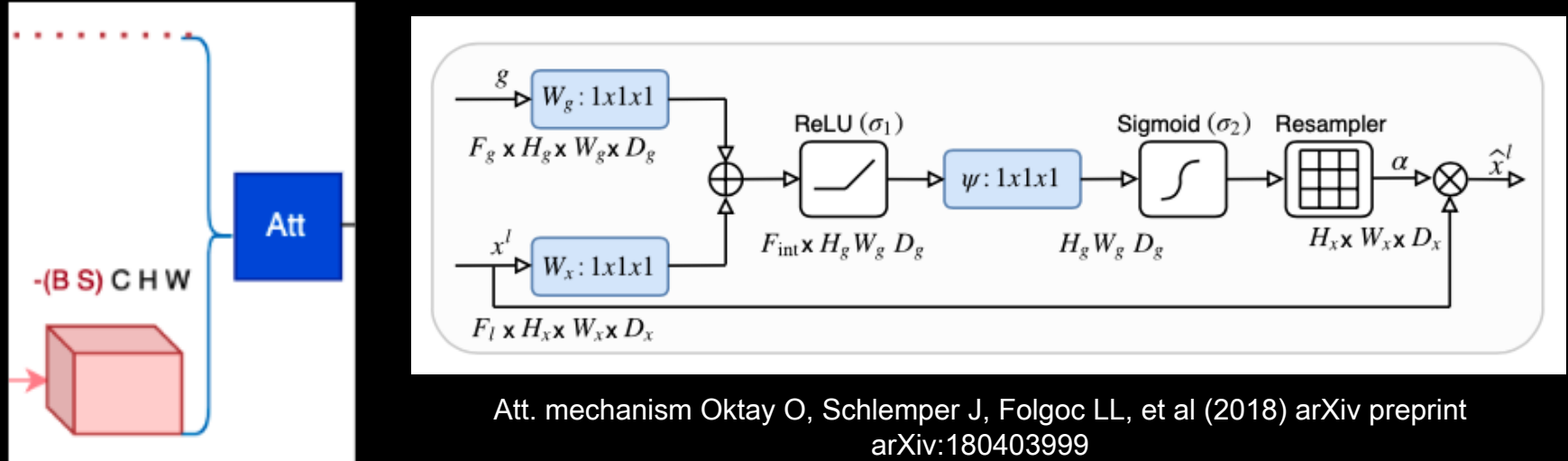


Broock, E. G., Asensio Ramos, A. & Felipe, T., 2022, (in preparation)

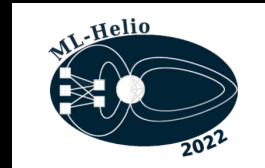


FarNet-II

Attention module: takes the skip connection and the current output and computes a mask that filters the skip connection that is finally applied to the decoder.



Snapshot from FarNet-II



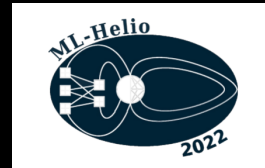
Cross-validation study

Training:

Inputs: 11 consecutive Carrington 24h phase-shifts maps (12h cadence).
Section of 144x180 centered on the FS.

Expected values: binary STEREO masks of the same region, generated for FarNet's study. Direct farside information (unlike the previous training).





Cross-validation study

Training:

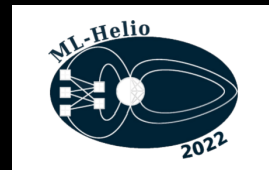
Inputs: 11 consecutive Carrington 24h phase-shifts maps (12h cadence).
Section of 144x180 centered on the FS.

Expected values: binary STEREO masks of the same region, generated for FarNet's study.

10 epochs, BS 10, dice loss, LR 3×10^{-4} .

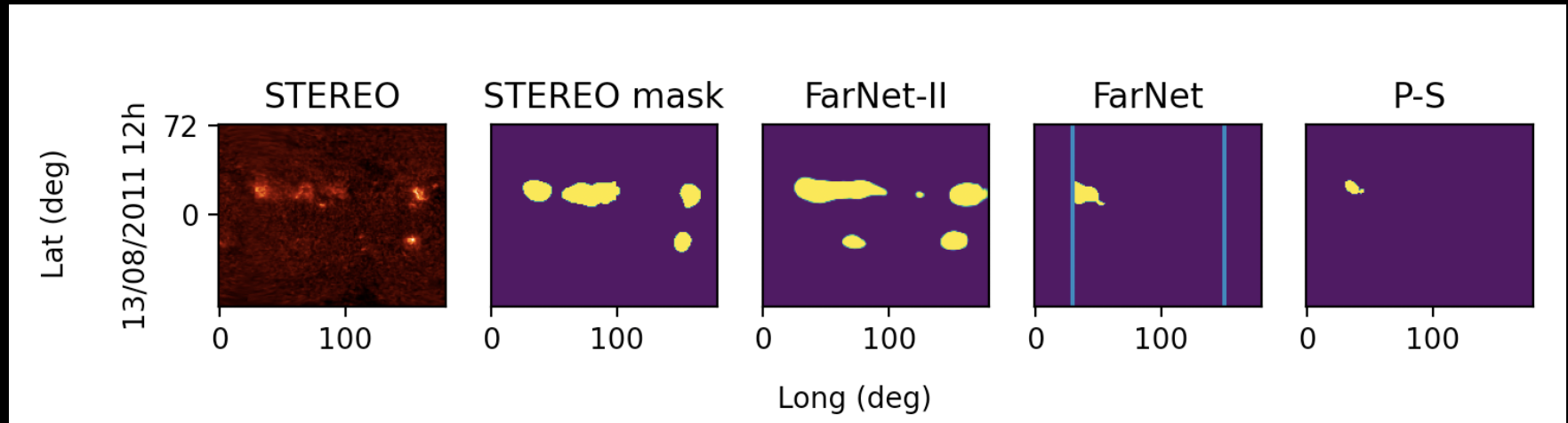
Limited number of input-output pairs: 2230.

Cross-validation study: 37 trainings leaving 60 out to evaluate. Results averaged.



Cross-validation study

Example:



Broock, E. G., Asensio Ramos, A. & Felipe, T., 2022, (in preparation)

Cross-validation study

Dice studied as a function of the **index** in the sequences of **11 elements**. Averaged among **37 validation sets**, each one with its trained network applied. **Recurrent nature** of the LSTM modules may have an impact on the **tendency** of the dice. Vertical bars: **standard deviation** among 37 evaluations.

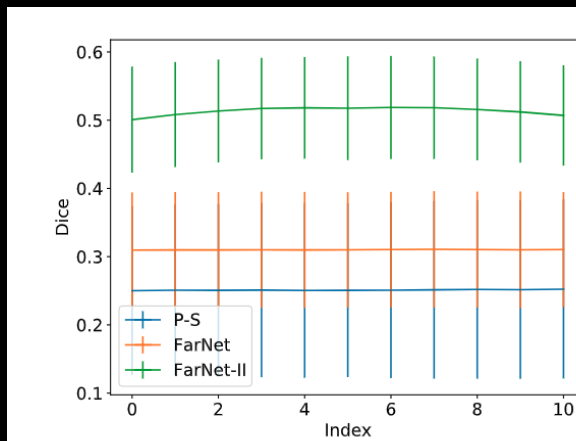


Fig. 3. Comparison among dice values for every method at study. Every region on outputs from FarNet with more than 5 contiguous pixels and a probability over 0.2 is taken into account.

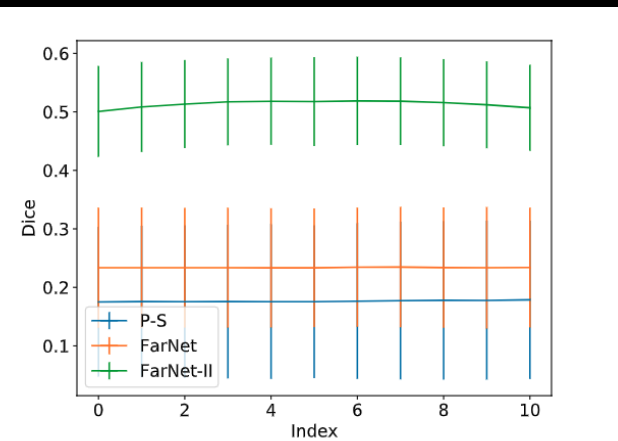
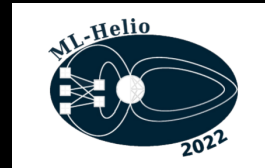


Fig. 4. Comparison among dice values for every method at study. Only regions with $P_i > 100$, for FarNet, and with $S > 400$, for the phase-sensitive method, are taken into account.



Cross-validation study

Compared with **FarNet** and the **phase-sensitive method**. FarNet and standard method contributions calculated from dices of every date that contributed to the prediction of each index for FarNet-II. Study restricted to the **common range** among the standard method, FarNet and FarNet-II.

Table 1. Means of the dice values of every sequence element, for each method and model, including variation on the filtering on outputs from FarNet and the phase-sensitive method.

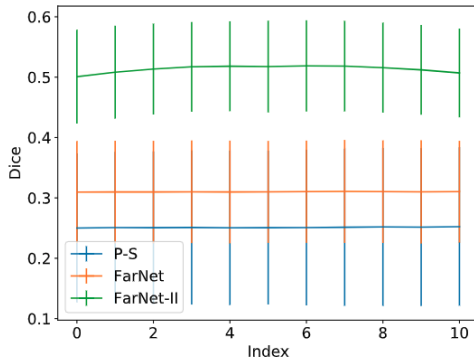


Fig. 3. Comparison among dice values for every method at study. Every region on outputs from FarNet with more than 5 contiguous pixels and a probability over 0.2 is taken into account.

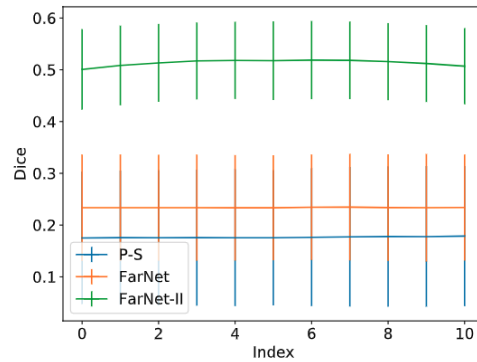


Fig. 4. Comparison among dice values for every method at study. Only regions with $P_i > 100$, for FarNet, and with $S > 400$, for the phase-sensitive method, are taken into account.

Ablation study

Comparison among ablated models, with only **unidirectional ConvLSTMs**, **without attention** and **without dropout**.

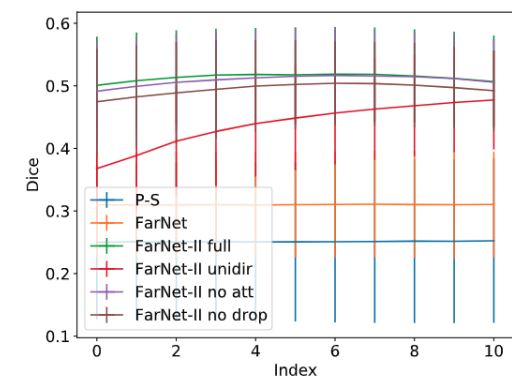


Fig. 7. Comparison among dice values for every method at study, including the ablated versions of FarNet-II. Every region on outputs from FarNet with more than 5 contiguous pixels and a probability over 0.2 is taken into account.

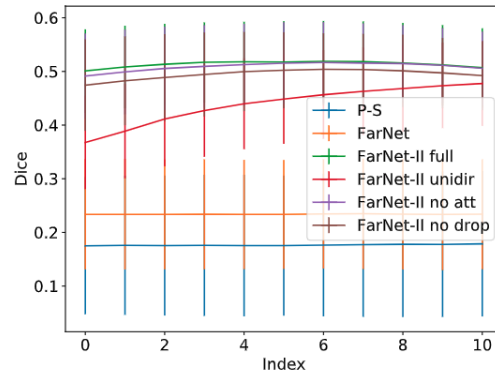
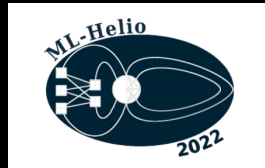


Fig. 8. Comparison among dice values for every method at study, including the ablated versions of FarNet-II. Only regions with $P_i > 100$, for FarNet, and with $S > 400$, for the phase-sensitive method, are taken into account.

Table 2. Means of the dice values of every sequence element for FarNet-II and its ablated models (U: unidirectional ConvLSTM; WA: without attention; WD: without dropout).

Method	Dice
FarNet-II	0.513
FarNet-II-U	0.438
FarNet-II-WA	0.501
FarNet-II-WD	0.495



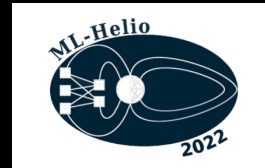
Open work and conclusions

Conclusions:

- FarNet-II is a U-net with attention mechanisms and bidirectional convolutional LSTM modules that outperforms FarNet and the phase-sensitive method for farside activity detection.
- We expect this model to be able to improve space weather predictions in the future.

Future work:

- Using FarNet-II to develop full magnetograms where every int value is a range in magnetic field (now just binary presence of activity).
- Full magnetogram predictions would be very valuable for space weather predictions.



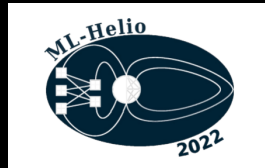
References

- Arge, C. N. et al. 2013, Solar Wind 13, 1539, 11
- Broock, E. G., Felipe, T., & Asensio Ramos, A. 2021, Astronomy & Astro-physics, 652, A132
- Broock, E. G., Asensio Ramos, A. & Felipe, T., 2022, (in preparation)
- Felipe, T. & Asensio Ramos, A. 2019, A&A, 632, A82
- Lindsey, C. & Braun, D. C. 2000a, Sol. Phys., 192, 261
- Lindsey, C. & Braun, D. C. 2000b, Science, 287, 1799
- Löptien, B. et al 2018, A&A, 619, A42
- Oktay O, Schlemper J, Folgoc LL, et al (2018) arXiv preprint arXiv:180403999
- X. Shi, Z. Chen, H. Wang, D. Y. Yeung, W. K. Wong, and W. C. Woo, Advances in Neural Information Processing Systems, vol. 2015-January, pp. 802–810, 2015.

Web:

Phase-shift maps: <http://jsoc.stanford.edu/ajax/lookdata.html>

SARD: <http://jsoc.stanford.edu/data/farside/>



Thank you for your attention!

This work was supported by the State Research Agency (AEI) of the Spanish Ministry of Science, Innovation and Universities (MCIU) and the European Regional Development Fund (FEDER) under grant with reference PGC2018-097611-A-I00 and by Consejería de Economía, Conocimiento y Empleo del Gobierno de Canarias and the European Regional Development Fund (ERDF) under grant with reference PROID2020010059.

